ACS POLYMERS Au
AN OPEN ACCESS JOURNAL OF THE AMERICAN CHEMICAL SOCIETY



pubs.acs.org/polymerau
Article

# From Molecular Constraints to Macroscopic Dynamics in Associative Networks Formed by Ionizable Polymers: A Neutron Spin Echo and Molecular Dynamics Simulations Study

Chathurika Kosgallana, Sidath Wijesinghe, Manjula Senanayake, Supun S. Mohottalalage, Michael Ohl, Piotr Zolnierczuk, Gary S. Grest,* and Dvora Perahia*

Cite This: ACS Polym. Au 2024, 4, 149−156
Read Online

ACCESS | Metrics & More | Article Recommendations | Supporting Information

**ABSTRACT:** The association of ionizable polymers strongly affects their motion in solutions, where the constraints arising from clustering of the ionizable groups alter the macroscopic dynamics. The interrelation between the motion on multiple length and time scales is fundamental to a broad range of complex fluids including physical networks, gels, and polymer−nanoparticle complexes where long-lived associations control their structure and dynamics. Using neutron spin echo and fully atomistic, multi-million atom molecular dynamics (MD) simulations carried out to times comparable to that of chain segmental motion, the current study resolves the dynamics of networks formed by suflonated polystryene solutions for sulfonation fractions $0 \leq f \leq 0.09$ across time and length scales. The experimental dynamic structure factors were measured and compared with computational ones, calculated from MD simulations, and analyzed in terms of a sum of two exponential functions, providing two distinctive time scales. These time constants capture confined motion of the network and fast dynamics of the highly solvated segments. A unique relationship between the polymer dynamics and the size and distribution of the ionic clusters was established and correlated with the number of polymer chains that participate in each cluster. The correlation of dynamics in associative complex fluids across time and length scales, enabled by combining the understanding attained from reciprocal space through neutron spin echo and real space, through large scale MD studies, addresses a fundamental long-standing challenge that underline the behavior of soft materials and affect their potential uses.

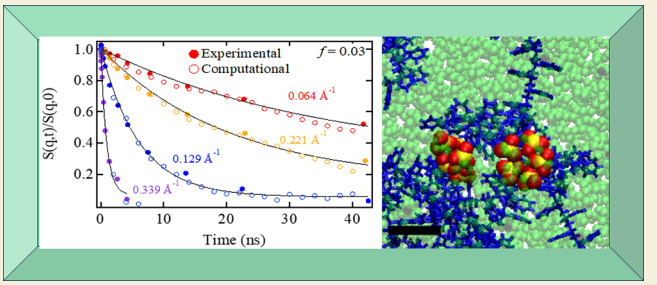


**KEYWORDS:** *ionomer solutions, suflonated polystryene, neutron spin echo, molecular dynamics simulations, exascale computing, dynamics*

## INTRODUCTION

The dynamic processes in networks of ionizable polymers drive their unique characteristics and enable their many current and potential applications in lightweight technologies ranging from clean energy generation and storage to biotechnology.[1−3] Their structure and dynamics in melts and solutions are governed by the coupling of two distinctive energy scales, van der Waals interactions and electrostatic forces, resulting in the coupling of responses on multiple length and time scales. Beyond ionizable polymeric networks, the coupling between processes that occur on distinctive length scales is a key to resolving the behavior of associative soft materials including networks, gels and nanoparticles-polymer hybrids as well as polymer-membrane complexes, all driven by dynamic constraints formed by physical association of chains.[4−9]

Ionizable polymers cluster into long-lived physical networks where the ionizable groups form long-lived assemblies, affecting both the segmental dynamics of the macromolecules and their ability to rearrange. Tethering a very small number of ionizable groups to the polymer backbone is sufficient to affect the motion of the polymer,[10,11] influencing their properties, including their mechanical response. Though the constraints of ionic clustering exerted on the motion of ionizable polymers are evident in their flow characteristics,[10,12] the molecular processes that underline the macroscopic lock-in of macromolecules is yet to be resolved.

Here, enabled by a conjunction of neutron spin echo (NSE) measurements and exascale atomistic molecular dynamics (MD) simulations, the dynamics of an ionizable model polymer, randomly sulfonated polystyrene (SPS), in solutions are probed across length and time scales. NSE is among the very few methods that can directly resolve dynamics on the mesoscopic length scale ca. 1−15 nm.[13−15] Large scale

Received: December 11, 2023
Revised: February 2, 2024
Accepted: February 6, 2024
Published: February 22, 2024

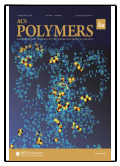





https://doi.org/10.1021/acspolymersau.3c00049
ACS Polym. Au 2024, 4, 149−156

atomistic MD simulations, that capture the time scales of the actual relaxation times of the chains, provide real-space insight,[16,17] enabling the translation of knowledge across time length scales.

The correlation between the ionic cluster characteristics and the overall properties of ionizable polymers stems from the balance of the chain elasticity, or pull-out forces, and that of ionic electrostatic interactions as was postulated by Eisenberg and co-workers,[18−21] Dreyfus,[22] and Mauritz.[23] The pioneering observation of Weise and co-workers.[24−29] who demonstrated that a small number of ionizable groups tethered to the polystyrene backbone results in a strong increase in the viscoelastic response that differs significantly from that of short, nonentangled flexible van der Waals polymers, has driven the quest to resolve the pathways in which clustering affects the dynamics of ionizable polymers in melts and in solutions. This impact, as reflected in the dynamic structure factor $S(q,t)$ and shear viscosity, was captured by Agrawal et al. using MD simulations.[17] They showed that in melts, dynamics of the polymer depends on the counterion and cluster morphology. A direct correlation between flow response and clustering has been recently demonstrated, where the flow viscosity is directly impacted by the size, shape and distribution of the clusters.[12,30]

Early NSE studies of SPS with low sulfonation levels in THF and DMSO solvents resolved the polymer relaxation time in terms of a correlation length $\xi$ that captures interchain correlations.[31] These studies have provided a glimpse into the correlation of chain relaxation and viscosity, providing the knowledge base that underlies the current studies. Further studies probed SPS in toluene at the low sulfonation regime and high molecular weight showed that even at concentrations as low as 1% the ionic clusters have a large impact on polymer motion on the nanosecond time scale.[32] Our recent quasi elastic neutron scattering (QENS) studies have shown that the dynamics of SPS in its acid form, in cyclohexane, a poor solvent for both the backbone and the sulfonated groups at room temperature, is constrained on the length scale of the rigid segment of the polymer, the length scale accessible to QENS. This motion increases with increasing temperature with a distinctive transition to a faster dynamics at the $\theta$ temperature of the polystyrene backbone in cyclohexane.[33]

With results from real and reciprocal space, the current study strives to correlate the effects of clustering on the translation of constraint dynamics from the atomistic level and segmental length scales to the overall motion of the polymers, using suflonated polystyrene in the ionomer regime. SPS in its ionomer regime, where well-defined clusters are formed, is a well-studied polymer whose synthetic routes lead to narrow molecular weight distribution and the degree of sulfonation can be controlled. The study focuses on short, lightly sulfonated SPS with low molecular weights of ∼11 kg/mol in toluene which is a good solvent for the polystyrene backbone. The small number of ionizable groups tethered to the backbone is sufficient to form clusters that constrain macroscopic motion, as shown by rheology, while the polymer backbone remains dynamic.

The experimental studies were carried out on the acid form and the computational studies with $Na^+$ counterions with the goal of understanding the effect of clustering on constraint chain dynamics on the mesoscopic length scale, independent of the specific composition of the ionic domains. The internal electrostatic characteristics of clusters are governed by packing of charges, as shown theoretically by Dreyfus[22] and is strongly affected by the valency of the cation. In solutions, the $SO_3^-$ groups could be driven into clusters by several factors including the gain in electrostatic energy and the low solvent affinity to both the SPS backbone and ionic groups. The degree of condensation of the counterion depends on the inherent ionic characteristics of each of the counterions as well as residual humidity trapped in the system.

## METHODOLOGY

Sulfonated polystryrene in its acid form with a molecular weight of ∼11 kg/mol with a polydispersity index of 1.2 was purchased from Polymer Source Inc. The polymer was synthesized by anionic polymerization and was randomly sulfonated to sulfonation fractions of $f$ = 0.03 and 0.09 of the available sites. Samples were made by dissolving 10 wt % of the polymer in $d$-toluene purchased from Cambridge Isotope Laboratories, Inc., USA. At these low concentrations, the polymer readily dissolves. Samples were then allowed to equilibrate for several days under ambient conditions. The polymer concentration is typical of that used in solution casting of ionic polymers and above the overlap concentration (∼6.4 wt %) of the polystyrene with similar molecular weights.

### SANS Measurements

SANS experiments were carried out on the General-Purpose Small Angle Neutron Scattering (GP-SANS) at the High Flux Isotope Reactor, Oak Ridge National Laboratory.[34,35] Data were collected at three detector-to-sample distances of 1.1, 4.8, and 19.2 m to capture the momentum transfer $q$ = 0.005−0.7 $Å^{-1}$ using a wavelength of $\lambda$ = 4.75 Å, with $\Delta\lambda/\lambda$ of 13%, where $q = 4\pi\sin(\theta)/\lambda$. $I(q)$ was recorded for the solutions, empty cell, standard, and $d_8$-toluene. Samples were encapsulated in a 2 mm thick banjo Hellma cells.

### Neutron Spin Echo

NSE experiments were performed at the spallation neutron source (SNS, Oak Ridge, TN, USA).[13] Data from two neutron wavelengths 8 and 11 Å were combined to cover a wide $q$-range of 0.057 to 0.32 $Å^{-1}$ and Fourier times of 0.04−100 ns. The $q$ range and the Fourier time probed were determined by sample characteristics and instrument limits.

Two reference samples, a sheet of graphite and $Al_2O_3$ powder, were measured and used to correct for instrument resolution. The solvent was run separately and subtracted from the data. The data were collected by an in-house program, developed initially in Jülich Center for Neutron Science, Germany, and reduced to the form of $S(q,t)$ using DrSpine program.[36] The temperature was controlled at 303 K by an SP FTS ThermoJet control system (SP Industries Warminster, PA) with the accuracy of ±0.5 K. Samples were encapsulated in 3 mm thick quartz rectangular Hellma cells (Müllheim, Germany).

### Molecular Dynamics Simulations

Comparable systems were studied by MD simulations. Sulfonated polystyrene and toluene were built using the polymer builder in BIOVIA Materials Studio. Monomers of styrene were retrieved from the BIOVIA library. Some of these were sulfonated to form sulfonated styrene. Using the random polymerization mode and an atactic configuration, the two monomers were randomly tethered with a specified ratios of the two monomers to form chains with a given sulfonation fraction $f$. The system contained 148 unique, atatic sulfonated


https://doi.org/10.1021/acspolymersau.3c00049
ACS Polym. Au 2024, 4, 149−156

polystyrene chains with sulfonation fraction $f$ = 0, 0.03, and 0.09, each with a total molecular weight of ∼11 kg/mol with 106 monomer per chain with $Na^+$ as a counterion. Similar to the experiments, the computer solutions consist of 10 wt % polymer in toluene. Each system contains between 2.4 and 2.5 million atoms. The final dimension of the cell is $L \sim 31.0$ nm for the 3 values of $f$; dimensions that are much larger than the size of a polymer chain whose radius of gyration $R_g$ is 28−31 Å. The all atoms optimized potentials for liquid simulations (OPLS-AA) force fields, developed by Jorgensen et al.[37,38] were used to model the system. The initial simulations were carried out using the LAMMPS[39] software package and converted to GROMACS[40−42] for enhanced efficiency.

Each system was first run at constant pressure of 1 atm for 10 ns to obtain equilibrium density. The dielectric constant $\varepsilon$ was increased from 1 to 30 to reduce the residual electrostatic screening between ionic groups. This step breaks the ionic clusters allowing the chains to locally equilibrate. Each solution was run for 30 ns at constant volume after which the dielectric constant was reset to 1 and ran for 600−800 ns at temperature 300 K.

The molecular structure of sulfonated polystyrene together with the scattering lengths $b_i$ of each atom[43] used for the experimental and computational studies are given in Figure 1.

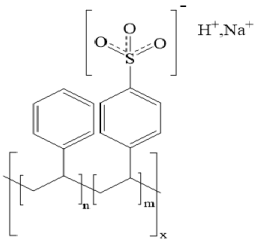


| Element/Isotope | Coherent scattering lengths $b_i$ ($10^{-15}$ m) |
|---|---|
| H | -3.74 |
| D | 6.67 |
| C | 6.65 |
| S | 2.80 |
| O | 5.80 |
| Na | 3.63 |

**Figure 1.** Chemical structure of SPS and the corresponding $b_i$ values for each of the atoms.

## RESULTS

SPS in toluene above the overlap concentration for polystyrene forms a network driven by concentration fluctuations and formation of clusters. The structure of SPS in melts and solutions have been studied by numerous groups.[16,44,45] An example of the small angle scattering (SANS) pattern of SPS with $f$ = 0.03 in toluene is given in Figure 2, where the very low

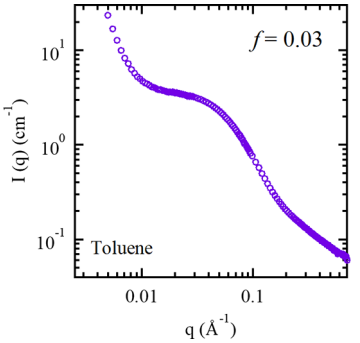


**Figure 2.** SANS patterns $I(q)$ versus $q$ for pronated 10 wt % SPS with $f$ = 0.03 in deuterated toluene at 303 K.

$q$ range depicts the signature of an instantaneous network and the intermediate $q$ range captures the signature of an interionic correlations, often referred to as the "ionic peak". Note that in contrast of SANS patterns of melts, for these low sulfonation levels, the interionic correlations are expressed in the line shape of the pattern.

The dynamic structure factor $S(q,t)$ at different wave vectors $q$ values as a function of time for a solution of $f$ = 0.03 in toluene, are presented in Figure 3. The lowest $q$ attainable on

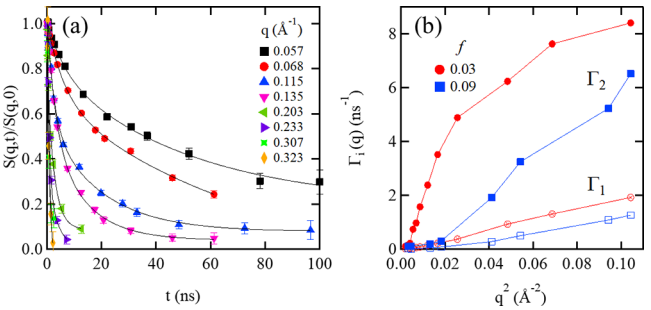


**Figure 3.** (a) Dynamic structure factor $S(q,t)$ from NSE for $f$ = 0.03 at 303 K as a function of $q$. The symbols correspond to the experimental data and the lines to the fit to a sum of two exponentials. (b) Effective diffusion coefficient $\Gamma_1(q)$ (open) and $\Gamma_2(q)$ (filled) extracted from the fits to a double exponential function for $f$ = 0.03 (red) and $f$ = 0.09 (blue).

the instrument, 0.057 $Å^{-1}$, captures the dimensions of correlations between ionic clusters in SPS melts and solutions. At these dimensions, $S(q,t)$ decreases significantly slower than at higher $q$ and does not fully decay within Fourier times accessible. For $q > 0.11$ $Å^{-1}$, where segmental dynamics is manifested, $S(q,t)$ fully decays within the time range accessible. This representation of $S(q,t)$ as a function of $t$ clearly shows that the overall decay is a result of multiple processes that characterize these clustered complex fluids. The fast dynamics is better observed in a presentation of $S(q,t)$ as a function of log $t$, as shown in Figure, S1. This representation of the data clearly shows that the contributions of the fast processes are $q$-dependent with low, intermediate, and high $q$ characteristic behavior.

A single exponential and a Kohlrausch−Williams−Watts (KWW) stretched exponential were first attempted to fit the data but were unable to capture the entire $q$ range for any of the systems, except for the lowest $q$ measured, where the spectra do not fully decay within the time scale of the measurement. With the two domains polymer-rich and solvent-rich, a sum of two exponentials was able to capture $S(q,t)$ for all samples across the $q$ and $t$

$$S(q,t)/S(q,0) = A_1\exp(-t/\tau_1(q)) + A_2\exp(-t/\tau_2(q)) \quad (1)$$

where $A_1$ and $A_2$ are pre-exponentials that weighs the contributions of each of the processes in $S(q,t)$, $t$ is time, and $\tau_1$ and $\tau_2$ are relaxation times. The sum of $A_1 + A_2 \rightarrow 1$ for all $q$.

The results obtained by fitting $S(q,t)$ to a sum of two exponential and the relaxation times are extracted. The relaxation rates $\Gamma_1(q)$ and $\Gamma_2(q)$, with $\Gamma_i(q) = 1/\tau_i(q)$, plotted in Figure 3b, are on the same order of magnitude, with $\Gamma_1(q) < \Gamma_2(q)$. However, both are essential to capture the relaxation of


https://doi.org/10.1021/acspolymersau.3c00049
ACS Polym. Au 2024, 4, 149−156

the polymer in toluene across the entire $q$ range. For the slower relaxation rate, $A_1$ = 0.78 at $q$ = 0.057 Å$^{-1}$ decreases to 0.39 at $q$ = 0.323 Å$^{-1}$ whereas for the faster one, $A_2$ increases from 0.22 to 0.60 across this $q$ range for $f$ = 0.03. For $f$ = 0.09, the slow relaxation rate, $A_1$ = 0.83 at $q$ = 0.057 Å$^{-1}$ decreases to 0.30 at $q$ = 0.323 Å$^{-1}$ whereas for the fast relaxation rate, $A_2$ increases from 0.17 to 0.70 across this $q$ range. The values of $A_1$ and $A_2$ are summarized in Figure S2 for all solutions measured by NSE.

For a simple, nonconstraint process the relaxation rates $\Gamma_i(q)$ vary linearly with $q^2$. However, $\Gamma_i(q)$ as a function of $q^2$ clearly deviates from linearity, as seen in Figure 3b, pointing to constraint dynamics. For diffusive systems, the extracted $\Gamma_i$ values are commonly plotted in terms of "effective diffusion" $\Gamma_i(q)/q^2$ as shown in Figure S3, demonstrating that in contrast to diffusive motion the relaxation rates exhibit a strong $q$ dependence. With increasing $q$, $\Gamma_1(q)$, increases with a lower slope than $\Gamma_2(q)$ and crosses over to a faster motion at $q$ = 0.135 Å$^{-1}$. Notable differences are observed between $f$ = 0.03 and 0.09 solutions, where the relaxation rates of $f$ = 0.03 solution is faster than that of $f$ = 0.09 across the entire $q$ range. With increasing $q$, $\Gamma_2(q)$ first increases slightly followed by a cross over to a rapid change that transitions to a slower increase at high $q$.

These results depict two interdependent dynamic processes, a slow motion that takes place on the length scale of the inter ionic-cluster correlation and a faster segmental motion that exhibits a strong $q$ dependence that diverges from simple diffusion, indicative of constraints motion of the chains beyond the mesoscopic length scale of the inter cluster correlation.

In these solutions, SPS whose backbone below the entanglement length of PS in the melt, constitute only 10% of the solution. The rest is toluene, which is good for the PS backbone. Therefore, beyond the effects of concentration fluctuations at these polymer concentrations, the constraint dynamics is expected to arise from direct confinement of segments to the ionic clusters and bridging between clusters through individual chains residing in several clusters simultaneously.

Visualization of computed solutions of PS and SPS with $f$ = 0, 0.03, and 0.09 are shown in Figure 4. For all $f$ values, at 10 wt % the polymer in toluene the solutions are heterogeneous. Though toluene is a good solvent for polystyrene, 10 wt % of the polymer drive concentration heterogeneities with PS-rich and toluene-rich domains.

With increasing sulfonation to $f$ = 0.03, clusters are formed, enhancing the segregation of polymer-rich and solvent rich regions, where the polymer rich domains propagate across the solution. In the $f$ = 0.09 solutions, well-defined clusters are observed, and the polymer rich domains become denser and often segregated from the toluene. This significant phase segregation between the polymer-rich and solvent domains as has been previously reported by SANS.[44] This inherent inhomogeneous in these associative systems drives the complex dynamics observed in $S(q,t)$.

Visualization of representative chains in the solutions, shown in Figure 4b, captures the motion of the chains 5 ns apart for $f$ = 0, 0.03, and 0.09. The $Na^+$ counterions are condensed and do not move away from the ionic groups within the time scale observed. In this time frame, only the fast motion is visually captured, the large-scale breathing mode of the entire network is observed only through the change in the position of the clusters. The chain segments closer to the clusters however

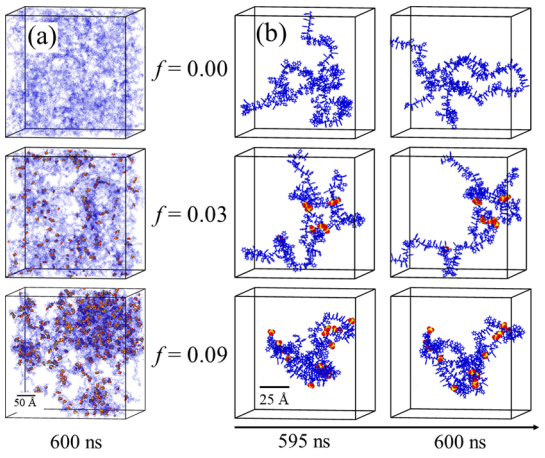


**Figure 4.** (a) Visualization of polymer domains in solutions of $f$ = 0.00, 0.03 and 0.09, at 300 K. Toluene is removed for clarity. (b) Visualization of two chains in all solutions at 5 ns intervals with only 1/27 of the simulation cells shown (blue—backbone, red—oxygen, yellow—sulfur, black- Na).

show comparatively less motion than those further away and the overall chain mobility increases with their distance from the clusters.

The dynamic structure factor $S(q,t)$ was calculated for the computed solutions using

$$S(q,t) = \sum_{i,j=1}^{N} b_i b_j e^{iq\cdot(r_i(t)-r_j(t))} / \sum_{i=1}^{N} b_i^2 \quad (2)$$

where $b_i$ are the neutron scattering lengths of atom $i$ and $r_i(t)$ position of atom $i$ at time $t$. The dynamic structure factor for the computed solutions, in comparison with the experimentally measured spectra, are presented in Figure 5. The computed $S(q,t)$ for $f$ = 0.03 is compared with the corresponding experimental results in Figure 5a. The two are in distinctive agreement, which allows a direct correlation of the reciprocal space results with the molecular insight attained from computational studies. The computed $S(q,t)$ for the polymer, phenyl, and S rings of the SPS are shown for representative $q$ values in Figure 5b. As expected, for all three $q$ values, the dynamic structural factor of the nonsulfonated phenyl ring decays faster than the sulfonated and the polymer ring. The dynamic structure factor for the entire polymer follows the motion of the nonsulfonated ring. With increasing $q$, the phenyl ring motion shows higher deviation from the sulfonated one and the polymer motion. Similar trends have been previously obtained for SPS melts.[17] As $S(q,t)$ averages over clustered and nonclustered S-rings, together with coupling of the polymer backbone to the solvent, the differences in local dynamics of the S-rings and the rest of the chains are smaller. The effective diffusion constants extracted from the computed $S(q,t)$, shown in Figure 5c, follow the same trend as the experimental one for the entire polymer. The degree impact of the degree of clustering and their size is reflected in computed $S(q,t)$, where increasing sulfonation fraction results in slower decay as shown in Figure 6a. However, the effects vary with length scale. At low $q$, where the intercluster correlations and direct tethering of the chains dominate, the effect of $f$ is the largest and $S(q,t)$ for $f$ = 0.03 and 0.09 are distinctive. At intermediate $q$ ($q$ = 0.1 Å$^{-1}$), the dynamics of $f$ = 0.09 captures slower dynamics compared with that of $f$ = 0 and 0.03. As $q$


https://doi.org/10.1021/acspolymersau.3c00049
ACS Polym. Au 2024, 4, 149−156

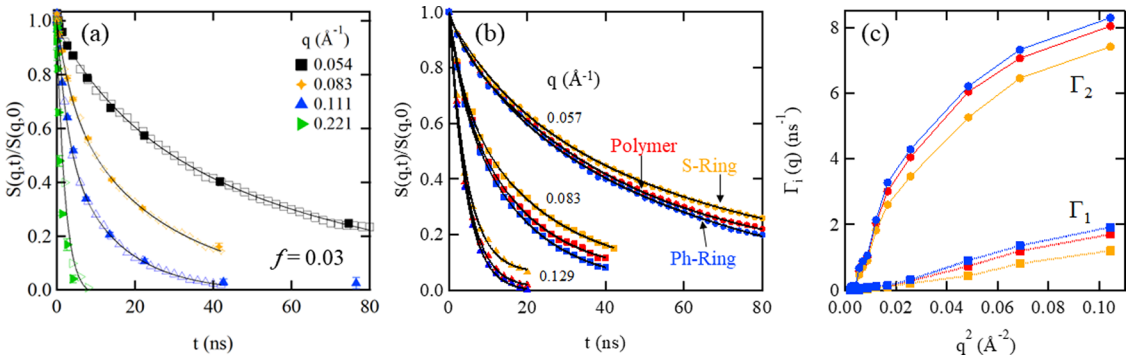


**Figure 5.** (a) Experimental (filled) and computed (open) $S(q,t)$ for $f = 0.03$. (b) Computed partial dynamic structure factors $S(q,t)$ of the indicated polymer segments. The solid lines in (a) and (b) correspond to the results of fitting to a sum of two exponents. (c) The relaxation rates $\Gamma_i(q)$ extracted from the fitting of the computed dynamic structure factors as a function of $q^2$ for the polymer (red), the phenyl rings (Ph-ring, orange) and the sulfonated phenyl rings (S-rings blue) for $f = 0.03$ solutions.

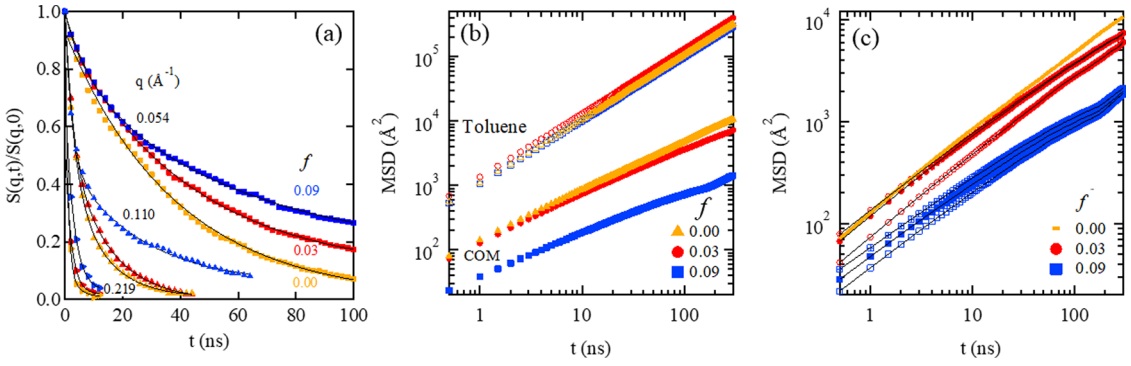


**Figure 6.** (a) $S(q,t)$ for the computed solutions at the indicated sulfonation fractions for $f = 0.00$, 0.03, and 0.09 at the indicated $q$ values. The solid lines are the results of fitting to the sum of two exponents, eq 1. (b) MSD of the center of mass as a function of time at the indicated sulfonation fractions (filled) and MSD of the toluene (open) in solutions at the indicated $f$ values. (c) MSD the polymer backbone marked by full symbols, the Ph-ring marked be empty ones, and S-Ring by a crossed symbol. The PS is marked by a line only.

increases, probing smaller dimensions, the motion the dynamics becomes faster where $f = 0.$ and 0.03 are hardly distinguishable and $f = 0.09$ is only slightly slower.

The corresponding presentation of $S(q,t)$ as a function of $\log(t)$ presented in Figure S4, shows that the fast processes are affected by the mesoscopic constraints for all $q$ values. This is indicative of several separate process including confinement within polymer-rich domains, segment that are directly confined to clusters as well as fully solvated chains. The motion of the entire chains is captured by the mean square displacement (MSD) of the center of mass (COM) of the polymers as shown in Figure 6b. The MSD clearly decreases with increasing sulfonation, where MSD of the nonsulfonated chain increases linearly with time, while that of $f = 0.03$ and 0.09 solutions curve toward leveling off at longer times, typical for constraint diffusion. This effect is further manifested in MSD of the separate constituents of the polymer, shown in Figure 4c where MSD of the sulfonated ring is slower than that of the nonsulfonated ones.

Comparing the motion depicted by MSD with segmental dynamics attained from NSE, translate the molecular insight into the mesoscopic length scale. For $f = 0.03$, the time for a monomer on the backbone to move an average distance of order $l = 2\pi/q$ is approximately the time it takes for $S(q,t)$ to decay by 90%. This indicates that decay times measured by the dynamic structure factor are dominated by the single chain relaxation. However, for $f = 0.09$, in the time $S(q,t)$ decays by 90%, the average distance a monomer on the backbone moves is much less than $2\pi/q$, indicating that the decay of $S(q,t)$ is dominated by the collection motion of the chains. For example, for $q = 0.011$ Å$^{-1}$, $l = 57$ Å, in the time for $S(q,t)$ to decay, the average displacement of monomers on backbone is ∼55 Å for $f = 0.03$ and ∼32 Å for $f = 0.09$. Similar behavior characterizes all $q$ values measured.

The polymer chains are confined to the network through clustering, however the network remains mobile and moves in the solvent, while polymer remains confined to the cluster. The number of distinctive, unique chains that participate in each of the clusters normalized to the number of sulfur atoms in a cluster $N_c$, is shown in Figure 7a. Sulfur atoms residing within 6 Å radius of each other are defined to be in the same cluster.[44] The average cluster size for $f = 0.03$ is 2.8 and for $f = 0.09$, it is 3.8. On average more than one chain associated with each cluster for clusters of size $N_c > 2$. Therefore, the clusters consist of sulfur groups from distinctive chains as well as intramolecular association. With the long-lived nature of these clusters, chains directly participate in more than one cluster driving macroscopic constraint motion. The clusters' "survival time" was measured by calculating the number $N_{pair}$ of pairs of sulfur atoms that remain in the same cluster as a function of time (Figure 7b). These results show that over times scale where $S(q,t)$ decays, the ionic clusters hardly change.

## CONCLUSIONS

The results attained from neutron spin echo studies and MD simulations, combing real and reciprocal space, have resolved a


https://doi.org/10.1021/acspolymersau.3c00049
ACS Polym. Au 2024, 4, 149−156

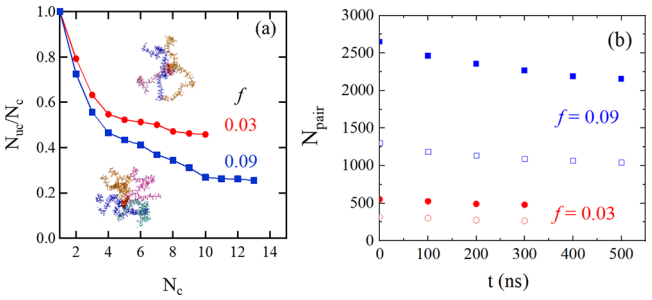


**Figure 7.** (a) Number of unique chains $N_{UC}$ normalized to the number of sulfur atoms $N_c$ in a cluster for $f = 0.03$ and 0.09, together with visualization of one cluster and the associated chains for each case. (b) Number of pairs $N_{pair}$ of sulfur atoms that remain in the same cluster as a function of time for all S pairs (filled) and for S pairs tethered to different chains (open).

long-standing critical challenge of how constraints exerted by assembly of limited number of ionic segments affects macroscopic dynamics in networks formed by ionizable polymer solutions. NSE and MD simulations were carried out on a model system of low sulfonation SPS in the acid and sodium salt respectively, in toluene. We show that SPS forms long-lived clusters of the ionizable groups, whose survival time is longer than microsecond, directly affecting the motion of the segments that are confined to the clusters. These clusters consist of ionizable groups that reside either on the same chain or on distinctive chains, where those who reside on different chains, constrain the dynamics on the mesoscopic length scale. Direct bridging between clusters, even by very few chains drive the larger scale constraint of the motion observed by rheology. Combining the results from real spaces and reciprocal space have enabled the realization of a long-standing challenge in polymers, an approach that will facilitate the understanding of complex systems and whose dynamics is coupled across time and length scales.

## ■ ASSOCIATED CONTENT

### Supporting Information

The Supporting Information is available free of charge at https://pubs.acs.org/doi/10.1021/acspolymersau.3c00049.

Supporting Information includes figures that present $S(q,t)$ vs log $(t)$, that are paired with the data presented in the body of the paper as $S(q,t)$ vs $t$. This representation of the data allows a better visualization of the fast processes in the system. The Supporting Information also includes a plot of the pre-exponential fitting parameters $A_1$ and $A_2$ as a function of $q$ for the experimental systems, described in the main text. It also includes a presentation of the effective diffusion coefficients $\Gamma_i(q)/q^2$ extracted from the fitting of the NSE data as a function of $q$. The different representation of the data in the main body of the manuscript and in the Supporting Information allowed a better insight into the multiscale dynamics of the system (PDF)

## ■ AUTHOR INFORMATION


### Corresponding Authors

**Gary S. Grest** − *Sandia National Laboratories, Albuquerque, New Mexico 87175, United States;* orcid.org/0000-0002-5260-9788; Email: gsgrest@sandia.gov

**Dvora Perahia** − *Department of Chemistry, Clemson University, Clemson, South Carolina 29634, United States; Department of Physics, Clemson University, Clemson, South Carolina 29631, United States;* orcid.org/0000-0002-8486-8645; Email: dperahi@g.clemson.edu

### Authors

**Chathurika Kosgallana** − *Department of Chemistry, Clemson University, Clemson, South Carolina 29634, United States*

**Sidath Wijesinghe** − *Department of Chemistry, Clemson University, Clemson, South Carolina 29634, United States; Department of Chemistry, Appalachian State University, Boone, North Carolina 26808, United States;* orcid.org/0000-0002-4812-1034

**Manjula Senanayake** − *Department of Chemistry, Clemson University, Clemson, South Carolina 29634, United States;* Present Address: Neutron Scattering Division, Oak Ridge National Laboratory, Oak Ridge, Tennessee 37831, USA; orcid.org/0000-0002-3139-0625

**Supun S. Mohottalalage** − *Department of Chemistry, Clemson University, Clemson, South Carolina 29634, United States;* Present Address: Materials Science Division, Lawrence Livermore National Laboratory, Livermore, California 94550, USA.

**Michael Ohl** − *Neutron Scattering Division, Oak Ridge National Laboratory, Oak Ridge, Tennessee 37831, United States;* Present Address: Research Center Jülich, 52428 Jülich, Germany.; orcid.org/0000-0002-8656-8005

**Piotr Zolnierczuk** − *Neutron Scattering Division, Oak Ridge National Laboratory, Oak Ridge, Tennessee 37831, United States*

Complete contact information is available at: https://pubs.acs.org/10.1021/acspolymersau.3c00049


### Notes

The authors declare no competing financial interest.

## ■ ACKNOWLEDGMENTS

D.P. gratefully acknowledges DOE grant DE-SC0019284 for support. NSE measurements were carried at ORNL's spallation neutron source. This research used resources at the Spallation Neutron Source, a DOE Office of Science User Facility operated by the Oak Ridge National Laboratory. The authors kindly acknowledge the use of computational resources provided by NSF MRI-1725573. This work was made possible in part by advanced computational resources deployed and maintained by Clemson Computing and Information Technology. This research used resources at the National Energy Research Scientific Computing Center (NERSC), a U.S. Department of Energy Office of Science User Facility operated under contract no. DE-AC02-05CH11231. This work was performed, in part, at the Center for Integrated Nanotechnologies, an Office of Science User Facility operated for the U.S. Department of Energy (DOE) Office of Science. Sandia National Laboratories is a multimission laboratory managed and operated by National Technology & Engineering Solutions of Sandia, LLC, a wholly owned subsidiary of Honeywell International, Inc., for the U.S. DOEs National Nuclear Security Administration under contract no. DE-NA-0003525. The views expressed in this article do not necessarily represent the views of the U.S. DOE or the United States Government. We thank Shalika Meedin for helpful discussions.

## REFERENCES


(1) Goyal, P.; Kusoglu, A.; Weber, A. Z. Coalescing Cation Selectivity Approaches in Ionomers. *ACS Energy Letters* **2023**, *8*, 1551−1566.

(2) Mardle, P.; Chen, B.; Holdcroft, S. Opportunities of Ionomer Development for Anion-Exchange Membrane Water Electrolysis: Focus Review. *ACS Energy Letters* **2023**, *8*, 3330−3342.

(3) Wang, J.; Wu, B.; Wei, P.; Sun, S.; Wu, P. Fatigue-free artificial ionic skin toughened by self-healable elastic nanomesh. *Nat. Commun.* **2022**, *13*, 4411.

(4) Shivers, J. L.; Sharma, A.; MacKintosh, F. C. Strain-Controlled Critical Slowing Down in the Rheology of Disordered Networks. *Phys. Rev, Lett.* **2023**, *131*, No. 178201.

(5) Jones, T. J.; Dupuis, T.; Jambon-Puillet, E.; Marthelot, J.; Brun, P.-T. Soft deployable structures via core-shell inflatables. *Phys. Rev. Lett.* **2023**, *130*, No. 128201.

(6) Lou, Y. Appetizer on soft matter physics concepts in mechanobiology. *Develop. Growth Differ.* **2023**, *65*, 234−244.

(7) Rao, A.; Olsen, B. D. Structural and dynamic heterogeneity in associative networks formed by artificially engineered protein polymers. *Soft Matter* **2023**, *19*, 6314−6328.

(8) Webber, M. J.; Tibbitt, M. W. Dynamic and reconfigurable materials from reversible network interactions. *Nature Rev. Mater.* **2022**, *7*, 541−556.

(9) Zhao, J.; Meng, F. Modeling Viscoelasticity and Dynamic Nematic Order of Exchangeable Liquid Crystal Elastomers. *Phys. Rev. Lett.* **2023**, *131*, No. 068101.

(10) Weiss, R.; Zhao, H. Rheological behavior of oligomeric ionomers. *J. Rheol.* **2009**, *53*, 191−213.

(11) Colby, R.; Zheng, X.; Rafailovich, M.; Sokolov, J.; Peiffer, D.; Schwarz, S.; Strzhemechny, Y.; Nguyen, D. Dynamics of lightly sulfonated polystyrene ionomers. *Phys. Rev, Lett.* **1998**, *81*, 3876−3879.

(12) Mohottalalage, S. S.; Kosgallana, C.; Meedin, S.; O'Connor, T. C.; Grest, G. S.; Perahia, D. Response of Sulfonated Polystyrene Melts to Nonlinear Elongation Flows. *Macromolecules* **2023**, *56*, 947−953.

(13) Ohl, M.; Monkenbusch, M.; Arend, N.; Kozielewski, T.; Vehres, G.; Tiemann, C.; Butzek, M.; Soltner, H.; Giesen, U.; Achten, R. The spin-echo spectrometer at the Spallation Neutron Source (SNS). *Nucl. Instrum. Methods Phys. Res., Sect. A* **2012**, *696*, 85−99.

(14) Zamponi, M.; Kruteva, M.; Monkenbusch, M.; Willner, L.; Wischnewski, A.; Hoffmann, I.; Richter, D. Cooperative Chain Dynamics of Tracer Chains in Highly Entangled Polyethylene Melts. *Phys. Rev. Lett.* **2021**, *126*, No. 187801.

(15) Arrighi, V.; Higgins, J. S. Local effects of ring topology observed in polymer conformation and dynamics by neutron scattering—A review. *Polymers* **2020**, *12*, 1884.

(16) Agrawal, A.; Perahia, D.; Grest, G. S. Clustering effects in ionic polymers: Molecular dynamics simulations. *Phys. Rev. E* **2015**, *92*, No. 022601.

(17) Agrawal, A.; Perahia, D.; Grest, G. S. Cluster morphology-polymer dynamics correlations in sulfonated polystyrene melts: computational study. *Physical review letters* **2016**, *116* (15), No. 158001.

(18) Eisenberg, A. Clustering of ions in organic polymers. *A theoretical approach. Macromolecules* **1970**, *3*, 147−154.

(19) Rigdahl, M.; Eisenberg, A. Viscoelastic properties of sulfonated styrene ionomers. *J. Polymer Science: Polymer Physics Edition* **1981**, *19*, 1641−1654.

(20) Eisenberg, A.; Hird, B.; Moore, R. A new multiplet-cluster model for the morphology of random ionomers. *Macromolecules* **1990**, *23*, 4098−4107.

(21) Eisenberg, A.; Kim, J. *Introduction to Ionomers*; John Wiley and Sons, Inc, 1998.

(22) Dreyfus, B. Model for the clustering of multiplets in ionomers. *Macromolecules* **1985**, *18*, 284−292.

(23) Mauritz, K. A. Review and Critical Analyses of Theories of Aggregation in Ionomers. *J. Macromolecular Sci. C* **1988**, *28*, 65−98.

(24) Lu, X.; Steckle, W.; Weiss, R. Ionic aggregation in a block copolymer ionomer. *Macromolecules* **1993**, *26*, 5876−5884.

(25) Weiss, R.; Yu, W.-C. Viscoelastic behavior of very lightly sulfonated polystyrene ionomers. *Macromolecules* **2007**, *40*, 3640−3643.

(26) Ling, G. H.; Wang, Y.; Weiss, R. Linear viscoelastic and uniaxial extensional rheology of alkali metal neutralized sulfonated oligostyrene ionomer melts. *Macromolecules* **2012**, *45*, 481−490.

(27) Qiao, X.; Weiss, R. A. Nonlinear Rheology of Lightly Sulfonated Polystyrene Ionomers. *Macromolecules* **2013**, *46*, 2417−2424.

(28) Zhang, L.; Brostowitz, N. R.; Cavicchi, K. A.; Weiss, R. Perspective: Ionomer research and applications. *Macromol. React. Eng.* **2014**, *8* (2), 81−99.

(29) Chen, Q.; Huang, C.; Weiss, R.; Colby, R. H. Viscoelasticity of reversible gelation for ionomers. *Macromolecules* **2015**, *48*, 1221−1230.

(30) Mohottalalage, S. S.; Senanayake, M.; Clemmer, J. T.; Perahia, D.; Grest, G. S.; O'Connor, T. Nonlinear elongation flows in associating polymer melts: from homogeneous to heterogeneous flow. *Phys. Rev. X* **2022**, *12*, No. 021024.

(31) Nyström, B.; Roots, J.; Higgins, J.; Gabrys, B.; Peiffer, D.; Mezei, F.; Sarkissian, B. Dynamics of polystyrene sulfonate ionomers in solution. A neutron spin-echo study. *J. Poly. Sci.Part C: Poly. Lett.* **1986**, *24*, 273−281.

(32) De Luca, E.; Waigh, T. A.; Monkenbusch, M.; Kim, J. S.; Jeon, H. S. Neutron spin echo study of the dynamics of micellar solutions of randomly sulphonated polystyrene. *Polymer* **2007**, *48*, 3930−3934.

(33) Mohottalalage, S. S.; Kosgallana, C.; Senanayake, M.; Wijesinghe, S.; Osti, N. C.; Perahia, D. Molecular Insight into the Effects of Clustering on the Dynamics of Ionomers in Solutions. *ACS Macro Lett.* **2023**, *12*, 1118−1124.

(34) Littrell, K.; Atchley, K.; Cheng, G.; Melnichenko, Y.; Wignall, G. General purpose small-angle neutron scattering instrument on HFIR Oak Ridge. *Neutron news* **2008**, *19*, 20−21.

(35) Wignall, G. D.; Littrell, K. C.; Heller, W. T.; Melnichenko, Y. B.; Bailey, K. M.; Lynn, G. W.; Myles, D. A.; Urban, V. S.; Buchanan, M. V.; Selby, D. L. The 40 m general purpose small-angle neutron scattering instrument at Oak Ridge National Laboratory. *J. Appl. Crystallogr.* **2012**, *45*, 990−998.

(36) Zolnierczuk, P.; Holderer, O.; Pasini, S.; Kozielewski, T.; Stingaciu, L.; Monkenbusch, M. Efficient data extraction from neutron time-of-flight spin-echo raw data. *J. Appl. Crystallography* **2019**, *52*, 1022−1034.

(37) Jorgensen, W. L.; Madura, J. D.; Swenson, C. J. Optimized Intermolecular Potential Functions for Liquid Hydrocarbons. *J. Am. Chem. Soc.* **1984**, *106*, 6638−6646.

(38) Jorgensen, W. L.; Maxwell, D. S.; TiradoRives, J. Development and testing of the OPLS all-atom force field on conformational energetics and properties of organic liquids. *J. Am. Chem. Soc.* **1996**, *118*, 11225−11236.

(39) Thompson, A. P.; Aktulga, H. M.; Berger, R.; Bolintineanu, D. S.; Brown, W. M.; Crozier, P. S.; in't Veld, P. J.; Kohlmeyer, A.; Moore, S. G.; Nguyen, T. D. LAMMPS-A flexible simulation tool for particle-based materials modeling at the atomic, meso, and continuum scales. *Comput. Phys. Commun.* **2022**, *271*, No. 108171.

(40) Berendsen, H. J.; van der Spoel, D.; van Drunen, R. GROMACS: A message-passing parallel molecular dynamics implementation. *Computer physics communications* **1995**, *91*, 43−56.

(41) Abraham, M. J.; Murtola, T.; Schulz, R.; Páll, S.; Smith, J. C.; Hess, B.; Lindahl, E. GROMACS: High performance molecular simulations through multi-level parallelism from laptops to supercomputers. *SoftwareX* **2015**, *1*, 19−25.

(42) Pronk, S.; Pall, S.; Schulz, R.; Larsson, P.; Bjelkmar, P.; Apostolov, R.; Shirts, M. R.; Smith, J. C.; Kasson, P. M.; van der Spoel, D.; et al. GROMACS 4.5: a high-throughput and highly parallel open source molecular simulation toolkit. *Bioinformatics* **2013**, *29*, 845−854.




https://doi.org/10.1021/acspolymersau.3c00049
*ACS Polym. Au* 2024, 4, 149−156

(43) https://www.ncnr.nist.gov/resources/n-lengths/ (accessed December 15, 2023).
(44) Kosgallana, C.; Senanayake, M.; Wijesinghe, S.; Mohottalalage, S.; He, L.; Grest, G. S.; Perahia, D. Clustering Effects on the Structure of Ionomer Solutions: A Combined SANS and Simulations Study. *Macromolecules* 2024, DOI: 10.1021/acs.macromol.3c01646
(45) Mohottalalage, S. S.; Aryal, D.; Thurston, B. A.; Grest, G. S.; Perahia, D. Effects of ionic group distribution on the structure and dynamics of amorphous polymer melts. *Macromolecules* **2022**, *55*, 217−223.



https://doi.org/10.1021/acspolymersau.3c00049
*ACS Polym. Au* 2024, 4, 149−156